

Modelling Annual Scintillation Velocity Variations of FRB 20201124A

R. A. Main¹★, S. Bethapudi¹, V. R. Marthi², M. L. Bause¹, D. Z. Li⁴, H.-H. Lin^{5,6},
L. G. Spitler¹, R. S. Wharton³,

¹Max-Planck-Institut für Radioastronomie, Auf dem Hügel 69, D-53121 Bonn, Germany

²National Centre for Radio Astrophysics, Tata Institute of Fundamental Research, Post Bag 3, Ganeshkhind, Pune - 411 007, India

³NASA Postdoctoral Program Fellow, Jet Propulsion Laboratory, California Institute of Technology, Pasadena, CA 91109, USA

⁴Cahill Center for Astronomy and Astrophysics, MC 249-17 California Institute of Technology, Pasadena CA 91125, USA

⁵Institute of Astronomy and Astrophysics, Academia Sinica, Astronomy-Mathematics Building, No. 1, Sec. 4, Roosevelt Road, Taipei 10617, Taiwan, R.O.C

⁶Canadian Institute for Theoretical Astrophysics, 60 St. George Street, Toronto, ON M5S 3H8, Canada

Accepted XXX. Received YYY; in original form ZZZ

ABSTRACT

Compact radio sources exhibit scintillation, an interference pattern arising from propagation through inhomogeneous plasma, where scintillation patterns encode the relative distances and velocities of the source, scattering material, and Earth. In [Main et al. \(2022\)](#), we showed that the scintillation velocity of the repeating fast radio burst FRB20201124A can be measured by correlating pairs of burst spectra, and suggested that the scattering was nearby the Earth at ~ 0.4 kpc from the low values of the scintillation velocity and scattering timescale. In this work, we have measured the scintillation velocity at 10 epochs spanning a year, observing an annual variation which strongly implies the screen is within the Milky Way. Modelling the annual variation with a 1D anisotropic or 2D isotropic screen results in a screen distance $d_l = 0.24 \pm 0.04$ pc or $d_l = 0.37 \pm 0.07$ pc from Earth respectively, possibly associated with the Local Bubble or the edge of the Orion-Eridanus Superbubble. Continued monitoring, and using measurements from other telescopes particularly at times of low effective velocity will help probe changes in screen properties, and distinguish between screen models. Where scintillation of an FRB originates in its host galaxy or local environment, these techniques could be used to detect orbital motion, and probe the FRB’s local ionized environment.

Key words: transients: Fast Radio Bursts

1 Introduction

Fast radio bursts (FRBs) are a powerful probe of intervening plasma. The total electron content along their line of sight is contained in their dispersion measure, while inhomogeneities in electron density result in scattering and scintillation, often concentrated in regions of high electron density. Scintillation encodes the time delay of scattered paths, and the relative distances and velocities of the emitting source, Earth, and scattering surface ([Cordes & Rickett 1998](#)).

Many repeating FRBs undergo periods of extreme activity (e.g. [Gajjar et al. 2018](#); [Li et al. 2019](#); [Nimmo et al. 2022a](#); [McKinven & Chime/Frb Collaboration 2022](#)). In [Main et al. \(2022\)](#) (hereafter M22A), we showed that in sufficiently active FRBs (ie. such that there are many burst pairs separated by \sim minutes), the scintillation timescale t_s can be measured through the pairwise correlation of bursts. From this, and the easily measured scintillation bandwidth ν_s , one can derive a scintillation velocity. As an extragalactic source, only the Earth’s velocity will matter for scintillation within the Milky Way, while the source’s velocity will matter if the screen is in the host galaxy.

In this paper, we measure the scintillation velocity of

FRB 20201124A over a full year, and we model the annual variation to determine the properties of the dominant scattering screen. We describe our data in Sec. 2 and our scintillation measurements in Sec. 3. In Sec. 4 we describe the annual scintillation model, and in Sec. 5 we discuss our conclusions and ramifications for future work.

2 Data

M22A focused on a single Effelsberg and uGMRT observation. We continued observing the source with Effelsberg and the uGMRT, with slightly different observing parameters described here.

The first Effelsberg observation on MJD 59313 used the PSRIX system ([Lazarus et al. 2016](#)), recording baseband in a contiguous 1210–1520 MHz band ([Hilmarsson et al. 2021](#)). One day later, many Effelsberg bursts were detected as part of the EVN campaign to localise the source ([Nimmo et al. 2022b](#)). All subsequent Effelsberg observation were made using the Effelsberg Direct Digitization system, recording baseband of the contiguous 1200–1600 MHz band. We restrict ourselves to the 200 MHz band 1270–1470 MHz throughout, to avoid sensitivity loss in the bandpass edges.

The first uGMRT observation on MJD 59309 used the beam of the incoherent array (IA) due to the uncertain source position, with 2048 channels across 550–750 MHz, and $655.36 \mu\text{s}$ time resolution

★ Email: ramain@mpifr-bonn.mpg.de

Table 1. Summary of all observations from which we had sufficient bursts to derive t_s . Observations marked with * were included in [Main et al. \(2022\)](#), with slightly different observing parameters as described in Section 2, and the observation labelled with † comes from the Effelsberg data from the observation used in the EVN localization ([Nimmo et al. 2022b](#)). The properties of the detected bursts will be analysed in further work.

MJD	T_{obs} (hr)	N_{burst}	ν_s (MHz)	t_s (min)	W (km/s/ $\sqrt{\text{kpc}}$)
Effelsberg (1270–1470 MHz)					
59313*	4	20	1.66 ± 0.1	17.7 ± 1.4	34.1 ± 2.9
59314†	3	13	1.06 ± 0.08	15.8 ± 1.0	30.5 ± 2.3
59478	4	9	1.39 ± 0.25	42.3 ± 4.3	13.0 ± 1.8
59611	3	53	1.27 ± 0.12	17.3 ± 0.8	30.5 ± 2.0
59612	5	49	1.56 ± 0.21	18.3 ± 1.0	31.9 ± 2.8
59624	4	12	1.64 ± 0.41	22.5 ± 3.8	26.6 ± 5.7
59655	2	7	1.8 ± 0.45	32.5 ± 9.0	19.3 ± 6.3
uGMRT (550–750 MHz)					
59310*	3	48	0.1 ± 0.01	7.0 ± 2.0	45.5 ± 14.4
59348	2	13	0.08 ± 0.01	5.7 ± 1.1	50.0 ± 10.5
59359	3	38	0.08 ± 0.01	5.2 ± 1.8	54.8 ± 21.8

([Marthi et al. 2022](#)). The source was quickly localized ([Nimmo et al. 2022b](#)), so subsequent observations used the phased array (PA), and our final data product was PA-1A beam, to greatly remove RFI. Additionally, these observations used 4096 channels, to better resolve the scintillation.

Bursts were searched for using PRESTO, as described in [Hilmarsen et al. \(2021\)](#); [Marthi et al. \(2022\)](#). We summarise our observing campaign, and burst detections in Table 2.

3 Scintillation Measurements

For each burst, we extract a spectrum identically to in M22A. At Effelsberg, we channelize the baseband data with 1024 channels, corresponding to 195.3125 kHz, while at uGMRT the channel size is 97.65625 kHz for the first and 48.828125 MHz for subsequent observations. For each observation, we then have N burst spectra $I(t_i, \nu)$ at discrete times t_i sampling the scintillation pattern unevenly in time (e.g. Fig. 1). We correlate each burst pair, giving a measure of $r(\Delta t_{ij}, \Delta \nu)$, with the error on each r_{ij} generated through MCMC method as described in M22A.

A Gaussian is fit to all values of $r(\Delta t_{ij}, \Delta \nu = 0)$, and the scintillation timescale t_s is the half width at half maximum (HWHM). To measure the scintillation bandwidth for each observation, we restrict ourselves only to bursts detected over more than half of the band. To account for frequency evolution, at Effelsberg we split the band into two, and at uGMRT in four, and fit each sub-band separately with a Lorentzian. The scintillation bandwidth ν_s is then the weighted sum of $\nu_{s,i} (\nu_{\text{band}}/\nu_{\text{ref}})^4$, and the error is the weighted error on the mean, referenced to 650 MHz at uGMRT and 1400 MHz at Effelsberg.

With enough burst pairs, a uniformly sampled 2D autocorrelation function (ACF) $R(\Delta t, \Delta \nu)$ can be constructed through the weighted sum of all burst pairs in bins of Δt . We show the ACF from MJD 59611 with 2 minute bins in Figure 2, along with cuts through $R(\Delta t, \Delta \nu = 0)$, $R(\Delta t = 0, \Delta \nu)$ and the Gaussian and Lorentzian corresponding the best fit scintillation timescale and bandwidth overplotted. The ACF cuts are fit well, although there is a clear tilt in the 2D ACF which is unaccounted for. Such tilts reflect a spatial asymmetry in the scattered power, likely reflecting local DM gra-

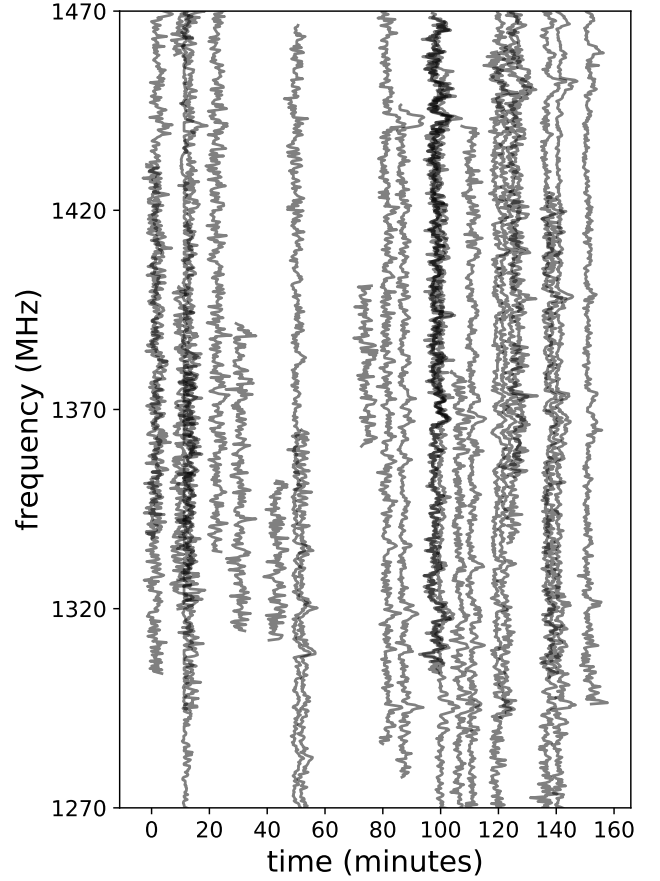


Figure 1. Dynamic spectrum from MJD 59611, the Effelsberg observation with the largest number of burst detections. The scintillation pattern of nearby bursts are evidently highly correlated.

dients in the screen ([Cordes et al. 2006](#); [Rickett et al. 2014](#)), and suggesting the screen is not isotropic.

As seen in pulsar giant pulses, nano- or micro-shots result in additional intrinsic spectral structure (e.g. [Bilous et al. \(2015\)](#)), and would reduce the expected correlation of adjacent pulses to 1/3 ([Cordes et al. 2004](#); [Main et al. 2021](#)). The spectra of nearby bursts correlate at $\sim 100\%$, suggesting there is no intrinsic spectral structure beyond the smooth burst envelope used for normalising the burst spectrum.

4 Annual Scintillation Model

In M22A, we used the expression for scintillation velocity from [Cordes & Rickett \(1998\)](#), which in the limit of an extragalactic source with $D \gg d_l$ (where D is the source distance, and d_l is the screen distance), the scintillation velocity V_{ISS} of a thin screen is related to ν_s, t_s as

$$W \equiv \frac{V_{\text{ISS}}}{\sqrt{d_l}} \approx 27800 \text{ km s}^{-1} \frac{\sqrt{2\nu_s}}{f t_s} \approx \frac{|\mathbf{v}_{\oplus} - \mathbf{v}_l|}{\sqrt{d_l}}, \quad (1)$$

with reference frequency f in GHz, ν_s in MHz, t_s in seconds, and where the scaled effective velocity W was defined for convenience, separating the unknowns from the measured values.

We consider two limiting cases of a fully anisotropic 1D screen, an isotropic 2D screen. We have full knowledge of \mathbf{v}_{\oplus} , so the only unknowns are the screen distance, and two parameters describing the

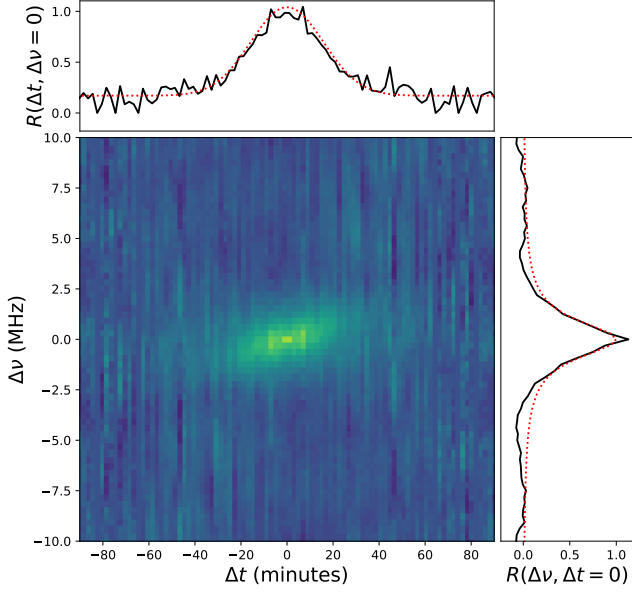


Figure 2. Image: 2D Autocorrelation function of the burst spectra from MJD 59611, slices through $\Delta\nu = 0$ (top panel) and $\Delta t = 0$ (right panel). The red lines show the model fit for scintillation timescale and bandwidth. There is a clear tilt in the ACF suggesting an asymmetric power distribution across the scattering screen (see Sec. 3)

Table 2. Results of the annual scintillation models, with parameters defined in Sec. 4.

Parameters	1D/anisotropic	2D/isotropic
d_l (kpc)	0.24 ± 0.04	0.37 ± 0.07
ψ ($^\circ$)	105 ± 15	–
v_ψ (km/s)	0.4 ± 0.5	–
$v_{l,ra}$ (km/s)	–	2.0 ± 1.0
$v_{l,dec}$ (km/s)	–	-8.0 ± 2.5
Reduced χ^2	1.13	0.67

geometry and velocity of the screen. For a 1D screen, we are only sensitive to the velocity parallel to the screen’s axis on the sky; the two unknowns are the screen axis ψ , and the screen velocity parallel to ψ , $v_{l,\psi}$,

$$W_{1D} = \frac{1}{\sqrt{d_l}} |v_{\oplus,ra} \sin(\psi) + v_{\oplus,dec} \cos(\psi) - v_{l,\psi}| \quad (2)$$

For a 2D, isotropic screen, the scintillation pattern is sensitive to the total transverse velocity, and the only additional unknown is the 2D velocity of the screen $v_{l,ra}$, $v_{l,dec}$,

$$W_{2D} = \frac{1}{\sqrt{d_l}} \sqrt{(v_{\oplus,ra} - v_{l,ra})^2 + (v_{\oplus,dec} - v_{l,dec})^2}. \quad (3)$$

We predict Earth’s velocity vector in right ascension and declination towards FRB 20201124A using SCINTOOLS (Reardon 2020). We fit our data using a Markov chain Monte Carlo (MCMC), using EMCEE, with uniform priors on the screen parameters. The results of our model fitting are shown in Figure 3, the posteriors shown in Figure 4, and best fit parameters are in Table 2.

4.1 Screen Association

Both the 1D and 2D model fit the data well, with reduced χ^2 of 1.13 and 0.67 respectively. While the 2D isotropic model is slightly

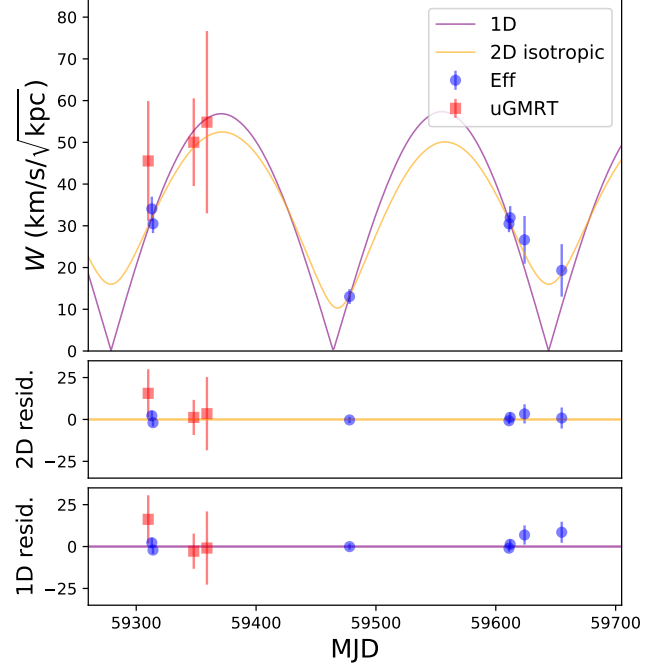


Figure 3. Measurements of the scintillation velocity, and the best fit 1D and 2D annual models (top), and residuals from the 2D (top) and 1D fit (bottom).

preferred, The ACFs are tilted, suggesting local DM slopes and screen anisotropies which are not accounted for; a general anisotropic screen model with screen axis and axial ratio could also be used, but the reduced χ^2 value less than 1 for the isotropic model already suggests that the model is overconstrained. The annual variation conclusively places the screen in the local region of the Milky Way, with screen distances of $d_{l,1D} = 0.24 \pm 0.04$ kpc and $d_{l,2D} = 0.37 \pm 0.07$ kpc.

Recent studies of pulsar scintillation have suggested scintillation near the local bubble boundary, including the dominant screen of PSR J1643-1224 located in the HII region Sh 2-27 ionized by ζ Oph (Mall et al. 2022). The edge of the Local Bubble hosts many star forming regions (Zucker et al. 2022), and provides a natural location for dense, ionized gas. To investigate this connection, we compare our screen constraints to a map of the local bubble in Lallement et al. (2019) derived from GAIA and 2MASS dust extinction (Fig. 5). Pelgrims et al. (2020) use this same map to model the inner edge of local bubble boundary; towards FRB 20201124A, the inner edge of this model is at a distance of 156 pc. This is slightly closer than our solutions but within 2σ of our derived lens distance from our 1D screen. Furthermore, the local bubble is not a sharp edge, as can be seen from the clear overdensity extending from $\sim 150 - 400$ pc along this sightline, suggesting a probable association of the scattering screen with the local bubble.

This sightline also passes near the edge of the Orion-Eridanus superbubble, a large $\sim 20^\circ \times 45^\circ$ expanding shell at a distance ~ 400 pc, ionized by UV radiation, and driven by supernovae and stellar winds from the Orion OB association (Ochsendorf et al. 2015; Tahani et al. 2022). This would also provide a natural location for plasma overdensities, and the distance roughly matches our screen estimates.

5 Conclusions and Future Avenues

We have modelled annual variation of the scintillation velocity in FRB 20201124A, deriving a screen distance which is coincident with the outer material in the local bubble. This adds to growing evidence

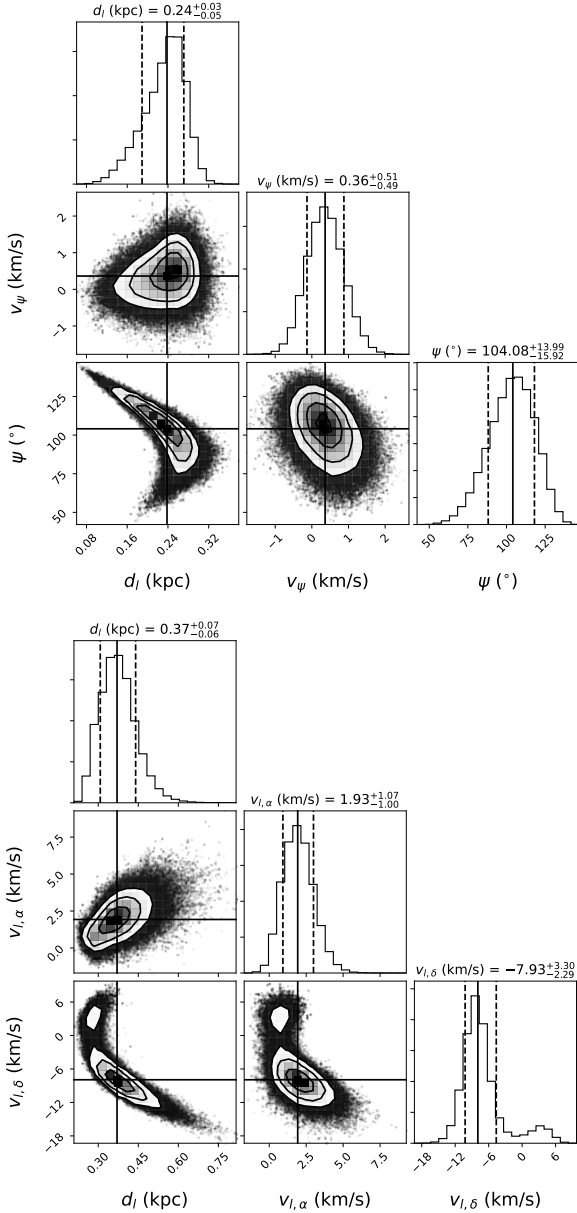


Figure 4. Posterior plots for the 1D (top) and 2D (bottom) annual models described in Sec. 4, plotted using CORNER.PY (Foreman-Mackey 2016). The contours show the 68% and 95% confidence intervals.

that the local bubble is often a significant contributor to interstellar scintillation (Mall et al. 2022; McKee et al. 2022; Stinebring et al. 2022; Sprenger et al. 2022). With a higher density of scintillation velocity measurements, particularly at the times of lowest effective velocity where the models are most different, the axial ratio and variable screen velocity could be constrained and the screen’s distance measured more precisely. In observations with even higher number densities of bursts, it will be possible to study scintillation using scintillation arcs (Stinebring et al. 2001), which probe substructure along the scattering screen, and are a more reliable measure of the relative velocities (e.g. Reardon et al. 2020).

It is often unknown a priori whether the scintillation screen originates in the Milky Way or the host galaxy of the FRB. A regular annual curve of scintillation velocity breaks this degeneracy. The scintillation screen can also be unambiguously constrained to the

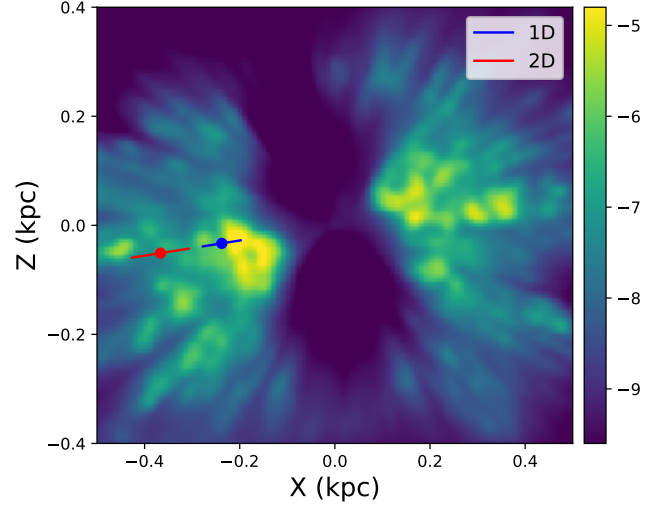


Figure 5. Screen constraints overlaid over an XZ slice through the local differential extinction map of Lallement et al. (2019), where the blue and red points show the screen distance constraints from our annual 1D and 2D models, respectively. The colorbar show the logarithmic differential extinction in magnitude/pc, and positive values of X point towards the galactic centre, and Z angles above and below the galactic plane. FRB 20201124A is only 1.88° of longitude away from the Galactic anticentre, motivating the choice of overplotting with the Y=0 slice.

Milky Way if there is a correspondence between scattering time and angular broadening measured through VLBI (Ocker et al. 2021). With new large-scale VLBI projects coming online, the scattering structures along thousands of sightlines could be constrained; combining all such results will lead to greatly improved models and understanding of the Galactic electron content (Cordes & Lazio 2002; Yao et al. 2017).

Many repeating FRBs have undergone periods of high activity, sufficient to perform similar scintillation analysis. These include FRB20121102A and FRB20180989B, both sources with periodic active windows (Rajwade et al. 2020; Cruces et al. 2021; Chime/Frb Collaboration et al. 2020), and variable magnetized local environments (Michilli et al. 2018; McKinven et al. 2022). FRB20190520B shows large magnetic field reversal (Anna-Thomas et al. 2022; Dai et al. 2022), and variable scattering on the timescale of minutes (Ocker et al. 2022). Such periodicities, and variable scattering and RM could be explained by an orbit with a windy companion star (Lin et al. 2021; Li et al. 2022), where an orbital dependence of scintillation velocity would be a smoking gun.

In cases with scintillation and scattering were present on different scales, it has been argued that scintillation would be quenched unless the two scattering screens obey an inequality such that each screen appears pointlike to the other (Masui et al. 2015; Cordes & Chatterjee 2019). However, in PSR B1508+55, Sprenger et al. (2022) found evidence of intertwined scintillation from 2 screens; the scintillation pattern of the screen nearby the source is imprinted onto the screen nearby the Earth, providing additional constraints on the geometry and extent of the scattering material. Incorporating these different propagation constraints will help in elucidating FRB host environments, and determining their progenitors.

ACKNOWLEDGEMENTS

RAM thanks Vincent Pelgrims for sharing their model of the local bubble surface. We thank the PRECISE team for sharing the dy-

namic spectra from the EVN localisation campaign. We thank the staff of the GMRT and Effelsberg who have made these observations possible. The Effelsberg 100-m telescope is operated by the Max-Planck-Institut für Radioastronomie. The GMRT is run by the National Centre for Radio Astrophysics of the Tata Institute of Fundamental Research. VRM acknowledges the support of the Department of Atomic Energy, Government of India, under project no. 12-R&D-TFR-5.02-0700. RSW is supported by an appointment to the NASA Postdoctoral Program at the Jet Propulsion Laboratory, administered by Oak Ridge Associated Universities under contract with NASA. Part of this research was carried out at the Jet Propulsion Laboratory, California Institute of Technology, under a contract with the National Aeronautics and Space Administration.

DATA AVAILABILITY

The data underlying this article will be shared on reasonable request to the corresponding author.

REFERENCES

- Anna-Thomas R., et al., 2022, arXiv e-prints, [p. arXiv:2202.11112](#)
- Bilous A. V., Pennucci T. T., Demorest P., Ransom S. M., 2015, *ApJ*, **803**, 83
- Chime/Frb Collaboration et al., 2020, *Nature*, **582**, 351
- Cordes J. M., Chatterjee S., 2019, *ARA&A*, **57**, 417
- Cordes J. M., Lazio T. J. W., 2002, arXiv e-prints, [pp astro-ph/0207156](#)
- Cordes J. M., Rickett B. J., 1998, *ApJ*, **507**, 846
- Cordes J. M., Bhat N. D. R., Hankins T. H., McLaughlin M. A., Kern J., 2004, *ApJ*, **612**, 375
- Cordes J. M., Rickett B. J., Stinebring D. R., Coles W. A., 2006, *ApJ*, **637**, 346
- Cruces M., et al., 2021, *MNRAS*, **500**, 448
- Dai S., et al., 2022, arXiv e-prints, [p. arXiv:2203.08151](#)
- Foreman-Mackey D., 2016, *Journal of Open Source Software*, **1**, 24
- Gajjar V., et al., 2018, *ApJ*, **863**, 2
- Hilmarsson G. H., Spitler L. G., Main R. A., Li D. Z., 2021, *MNRAS*, **508**, 5354
- Lallement R., Babusiaux C., Vergely J. L., Katz D., Arenou F., Valette B., Hottier C., Capitanio L., 2019, *A&A*, **625**, A135
- Lazarus P., Karuppusamy R., Graikou E., Caballero R. N., Champion D. J., Lee K. J., Verbiest J. P. W., Kramer M., 2016, *MNRAS*, **458**, 868
- Li D., Lin F. X., Main R., Pen U.-L., van Kerkwijk M. H., Yang I. S., 2019, *MNRAS*, **484**, 5723
- Li D., Bilous A., Ransom S., Main R., Yang Y.-P., 2022, arXiv e-prints, [p. arXiv:2205.07917](#)
- Lin F. X., Main R. A., Verbiest J. P. W., Kramer M., Shaifullah G., 2021, *MNRAS*, **506**, 2824
- Main R., Lin R., van Kerkwijk M. H., Pen U.-L., Rudnitskii A. G., Popov M. V., Soglasnov V. A., Lyutikov M., 2021, *ApJ*, **915**, 65
- Main R. A., Hilmarsson G. H., Marthi V. R., Spitler L. G., Wharton R. S., Bethapudi S., Li D. Z., Lin H. H., 2022, *MNRAS*, **509**, 3172
- Mall G., et al., 2022, *MNRAS*, **511**, 1104
- Marthi V. R., et al., 2022, *MNRAS*, **509**, 2209
- Masui K., et al., 2015, *Nature*, **528**, 523
- McKee J. W., Zhu H., Stinebring D. R., Cordes J. M., 2022, *ApJ*, **927**, 99
- McKinven R., Chime/Frb Collaboration 2022, The Astronomer's Telegram, **15679**, 1
- McKinven R., et al., 2022, arXiv e-prints, [p. arXiv:2205.09221](#)
- Michilli D., et al., 2018, *Nature*, **553**, 182
- Nimmo K., et al., 2022a, arXiv e-prints, [p. arXiv:2206.03759](#)
- Nimmo K., et al., 2022b, *ApJ*, **927**, L3
- Ochsendorf B. B., Brown A. G. A., Bally J., Tielens A. G. G. M., 2015, *ApJ*, **808**, 111
- Ocker S. K., Cordes J. M., Chatterjee S., 2021, *ApJ*, **911**, 102
- Ocker S. K., Cordes J. M., Chatterjee S., Li D., Niu C. H., McKee J. W., Law C. J., Anna-Thomas R., 2022, arXiv e-prints, [p. arXiv:2210.01975](#)
- Pelgrims V., Ferrière K., Boulanger F., Lallement R., Montier L., 2020, *A&A*, **636**, A17
- Rajwade K. M., et al., 2020, *MNRAS*, **495**, 3551
- Reardon D. J., 2020, Scintools: Pulsar scintillation data tools, Astrophysics Source Code Library, record ascl:2011.019 (ascl:2011.019)
- Reardon D. J., et al., 2020, *ApJ*, **904**, 104
- Rickett B. J., et al., 2014, *ApJ*, **787**, 161
- Sprenger T., Main R., Wucknitz O., Mall G., Wu J., 2022, *MNRAS*, **515**, 6198
- Stinebring D. R., McLaughlin M. A., Cordes J. M., Becker K. M., Goodman J. E. E., Kramer M. A., Sheckard J. L., Smith C. T., 2001, *ApJ*, **549**, L97
- Stinebring D. R., et al., 2022, arXiv e-prints, [p. arXiv:2207.08756](#)
- Tahani M., et al., 2022, *A&A*, **660**, L7
- Yao J. M., Manchester R. N., Wang N., 2017, *ApJ*, **835**, 29
- Zucker C., et al., 2022, *Nature*, **601**, 334

This paper has been typeset from a \LaTeX file prepared by the author.